

## IN MEDIUM $T$ -MATRIX WITH REALISTIC NUCLEAR INTERACTIONS\*

PIOTR BOŻEK AND PIOTR CZERSKI

H. Niewodniczański, Institute of Nuclear Physics  
Radzikowskiego 152, 31-342 Kraków, Poland

*(Received December 9, 2002)*

We calculate the self-consistent in-medium  $T$ -matrix for symmetric nuclear matter using realistic interactions with many partial waves. We find for the interactions used (CDBonn and Nijmegen) very similar results for on-shell quantities. The effective mass and the renormalization factor  $Z_F$  at the Fermi momentum are given for a range of densities.

PACS numbers: 21.65.+f

The presence of a strong interaction between nucleons at short distances requires the use of resummation methods for many-body calculations in nuclear matter. Besides the Brueckner–Hartree–Fock (BHF) summation of ladder diagrams [1,2] and advanced variational methods [3,4], the self-consistent in-medium  $T$ -matrix approach became feasible in last years [5–9]. The numerical method presented in [8] allows for efficient calculations using off-shell nucleon propagators with realistic interactions. Below we present results for the CDBonn [10] and Nijmegen potentials [11] incorporating all partial waves with total angular momentum  $J < 9$ . The in medium  $T$ -matrix [12]

$$T = V + VGGT \quad (1)$$

is calculated with the Green's function  $G = (\omega - p^2/2m - \Sigma)^{-1}$  self-consistently dressed by the self-energy in the  $T$ -matrix approximation

$$i\Sigma = \text{Tr}[T_A G]. \quad (2)$$

---

\* Supported by the Polish State Committee for Scientific Research (KBN), grant 2P03B02019.

The difference with respect to the BHF approach lies in the dressing of the Green's functions by the full spectral functions, which means off-shell propagation. Also, the double Green's function in the  $T$ -matrix equation represents the propagation of two particles or two-holes unlike in the Kernel of the Bethe–Goldstone equation in the BHF scheme where the Pauli-blocking factor forces the propagation of two particles always. The above equations are solved by iteration for several nuclear densities  $\rho$  in the range 0.2–2.4 normal nuclear densities  $\rho_0 = 0.16 \text{ fm}^{-3}$ . The details of the equations and numerics can be found in Refs. [7, 8].

We have improved the numerical algorithm to allow for many partial-waves in the  $T$ -matrix. We use a separable parameterization of the interaction, choosing 8 most important eigen-vectors of the interaction in the momentum representation for each uncoupled partial wave and 24 eigen-vectors for the coupled partial waves. This parameterization is essentially equivalent to the full parameterization in momentum. In previous  $T$ -matrix calculations a low-rank separable parameterization of the Paris potential was used. In this paper we compare the results for two realistic interactions without further simplifying approximations and taking many partial waves. With these calculations the binding energy and single-particle properties can be found without uncertainties due to technical simplifications.

The binding energy per particle in the  $T$ -matrix approach can be calculated from the Koltun's sum rule

$$\frac{E}{N} = \frac{1}{\rho} \int \frac{d^3p}{(2\pi)^3} \int_{-\infty}^{\mu} \frac{d\omega}{2\pi} \frac{1}{2} \left( \frac{p^2}{2m} + \omega \right) A(p, \omega), \quad (3)$$

where  $A$  is the nontrivial spectral function obtained for the dressed propagators. In fact any expression for the energy should give the same result, since the self-consistent  $T$ -matrix approximation is thermodynamically consistent [13]. The existence a generating function  $\Phi$  for the self-energy guarantees the fulfillment of thermodynamical relations between single-particle and global properties of the system. The fact that the  $T$ -matrix scheme is a consistent (conserving) approximation has been checked explicitly in [7] using a model interaction.

In the upper panels of Figs. 1 and 2 is shown the binding energy in the  $T$ -matrix approximation as a function of the density in symmetric nuclear matter compared to the corresponding BHF results. As noted previously the  $T$ -matrix gives smaller binding energies and smaller saturation densities than the BHF calculation. At low densities the BHF and the  $T$ -matrix results converge as expected. The interactions studied in this work give similar results, *e.g.* at normal nuclear density  $E/N = -14.3$  and  $-14.1$  MeV for the CDBonn and Nijmegen interaction, respectively. The corresponding

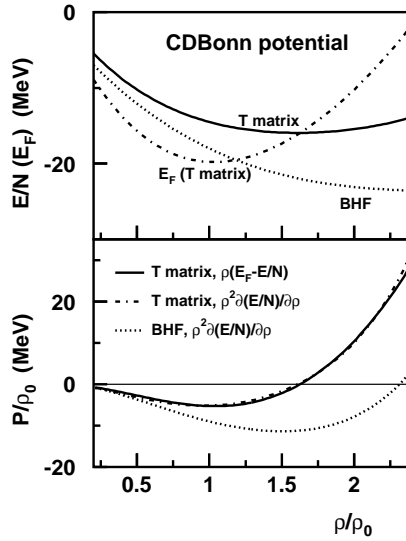


Fig. 1. Upper panel: The binding energy and the Fermi energy as a function of density for the  $T$ -matrix approach and the binding energy in the BHF calculation, all for the CDBonn potential. Lower panel: The pressure as a function of density obtained from two different expressions Eqs. (5) and (6). The solid and the dashed-dotted lines representing the two results for the pressure in the  $T$ -matrix calculation lie almost on top of each other.

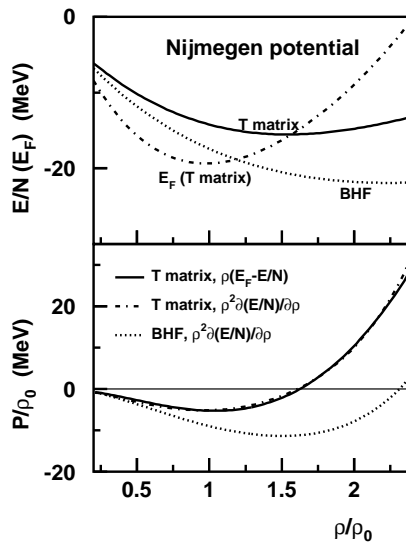


Fig. 2. Same as Fig. 1 but for the Nijmegen potential.

BHF binding energies at that density are 3.3–3.5 MeV lower. In the same figures the Fermi energy  $E_F$  is shown. The Fermi energy in the  $T$ -matrix calculation is consistent with the binding energy; the Hugenholtz–Van Hove relation [14]

$$E_F = \frac{E}{N} \quad (\text{at saturation density}) \quad (4)$$

is automatically fulfilled.

The pressure in the system can be obtained from several equivalent expressions. We consider

$$P = \rho^2 \frac{\partial(E/N)}{\partial\rho} \quad (5)$$

and

$$P = \rho \left( E_F - \frac{E}{N} \right). \quad (6)$$

From the second form follows the Hugenholtz–Van Hove relation at the saturation point ( $P = 0$ ). The expressions (5) and (6) are equivalent in the self-consistent  $T$ -matrix approximation. In the BHF approach the pressure can be calculated as the derivative of the binding energy (5).

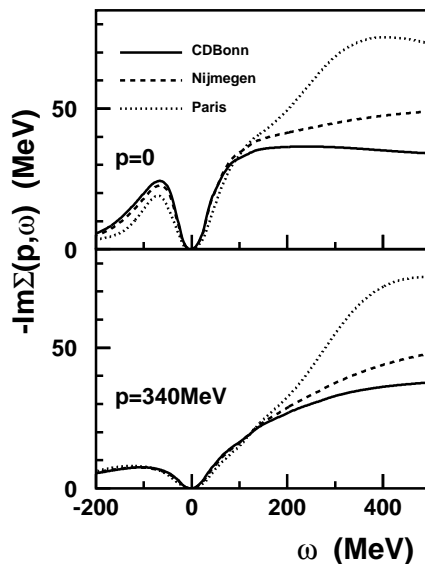


Fig. 3. The imaginary part of the retarded self-energy  $-\text{Im}\Sigma(p, \omega)$  as a function of the energy  $\omega$  for  $p = 0$  (upper panel) and  $p = 340$  MeV (lower panel) for different nucleon–nucleon potentials at  $\rho = \rho_0$ .

One-body properties are determined by the self-energy. In Fig. 3 is shown the imaginary part of the self-energy  $-\text{Im} \Sigma(p, \omega)$ . The self-energy is very similar for the CDBonn and Nijmegen potentials and close to the result for the Paris potential [8] for energies close to the Fermi energy ( $|\omega| < 200$  MeV) and for momenta up to 500 MeV. At higher energies differences start to appear, because of different off-shell behavior of the  $T$ -matrix for different interactions. The Paris interaction we use is a separable parameterization with a small number of partial waves, this can lead to additional differences as compared to results from the other two potentials.

As can be seen from Fig. 4 the self-energy on-shell, *i.e.* for  $\omega = \omega_p = p^2/2m + \text{Re} \Sigma(p, \omega_p)$ , is similar for different interactions. For momenta  $p < 700$  MeV the width of the quasiparticle excitation is similar. It is always zero at the Fermi momentum and increases quadratically when going away from it. The quadratic increase of the single-particle width is given by the cross section and the density of states at the Fermi surface. The cross sections are similar for different parameterizations of the nuclear potentials and the density of states at the Fermi surface is determined by the effective mass and the renormalization factor

$$Z_p = \left( 1 - \frac{\partial \text{Re} \Sigma(p, \omega)}{\partial \omega} \right)^{-1} \Big|_{\omega=\omega_p} . \tag{7}$$

As shown below, those quantities obtained for different nucleon–nucleon interactions are similar.

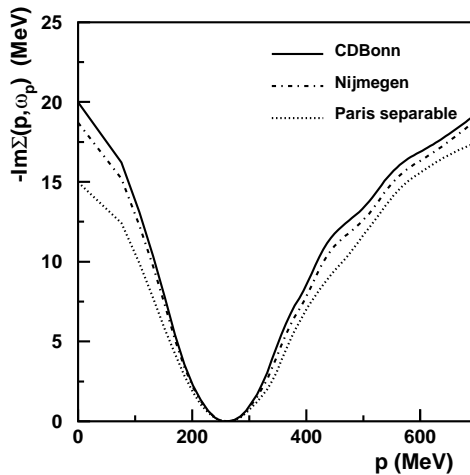


Fig. 4. The imaginary part of the retarded self-energy  $-\text{Im}\Sigma(p, \omega_p)$  at the quasiparticle pole as a function of the momentum ( $\rho = \rho_0$ ).

The real part of the self-energy determines the single-particle potential, *i.e.* the real part of the optical potential. The fulfillment of the Hugenholtz–Van Hove relation guarantees the correct normalization of the single-particle potential. The real part of the self-energy is given as the sum of the Hartree–Fock and dispersive contributions

$$\text{Re}\Sigma(p, \omega) = \Sigma_{\text{HF}}(p) + \int \frac{d\omega'}{\pi} \frac{\text{Im}\Sigma(p, \omega')}{\omega - \omega'}. \quad (8)$$

The Hartree–Fock part is different for the Nijmegen and CDBonn potentials, but the total single-particle energy on-shell is very similar (Fig. 5). The difference in the Hartree–Fock part is compensated by the dispersive part, which includes integration of the imaginary part of the self-energy far off-shell. The differences in  $\text{Im}\Sigma(p, \omega)$  for  $\omega > 200\text{MeV}$  (Fig. 3) give the necessary shifts leading to similar total optical potentials (8). Although the Nijmegen and CDBonn interactions show some differences in the off-shell behavior of the self-energies, the resulting properties of the quasiparticle pole are very similar in the range of densities  $\rho < 2\rho_0$ . The properties of the quasiparticles at the Fermi surface are defined by the renormalization factor (7) and the effective mass

$$m^* = \frac{pdp}{d\omega_p}. \quad (9)$$

The effective mass and the renormalization factor are important to define the effective interaction between quasiparticles [15, 16] and the superfluid

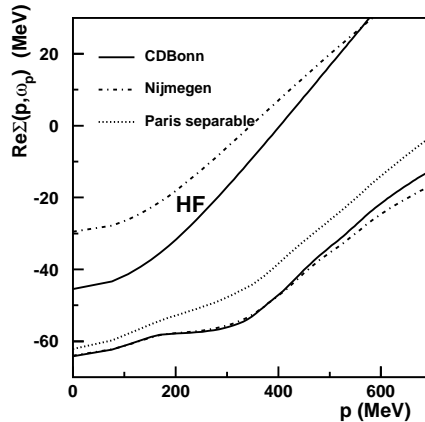


Fig. 5. The single-particle potential  $\text{Re}\Sigma(p, \omega_p)$  at the quasiparticle pole as a function of the momentum at  $\rho = \rho_0$ . The upper curves represent the Hartree–Fock contribution for the Nijmegen and CDBonn interactions.

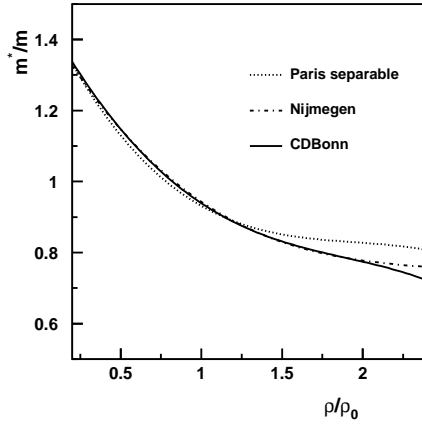


Fig. 6. The effective mass  $m^*/m$  at the Fermi surface for different nuclear interactions.

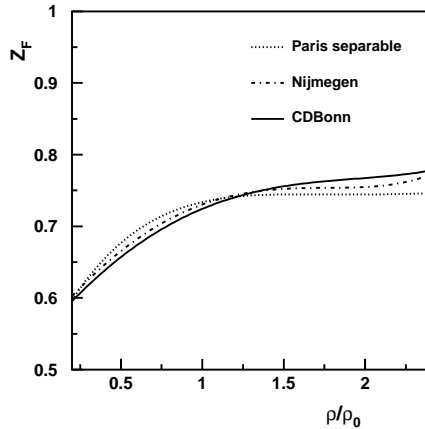


Fig. 7. The renormalization factor of the quasiparticle pole  $Z_p$  at the Fermi surface for different nuclear interactions.

gap [17, 18]. We present the calculation of these quantities for different interactions in a range of densities. We find that for  $\rho < 2\rho_0$  the CDBonn and the Nijmegen interactions give very similar results (Figs. 6, 7). The difference of the calculation using the separable Paris potential can be attributed to the simplicity of that parameterization. The effective mass in our calculation comes out very close to the free nucleon mass. It is useful for further applications to parameterize its density dependence

$$\frac{m^*}{m} = 1.43 - 0.623 \frac{\rho}{\rho_0} + 0.146 \left( \frac{\rho}{\rho_0} \right)^2 \quad (10)$$

and similarly the for renormalization  $Z_p$  at the Fermi momentum (Fig. 7)

$$Z_F = 0.57 + 0.2 \frac{\rho}{\rho_0} - 0.05 \left( \frac{\rho}{\rho_0} \right)^2 . \quad (11)$$

The above parameterizations of the density dependence of the effective mass and of the  $Z_F$  factor are valid in the range  $0.3\rho_0 < \rho < 2.6\rho_0$ . The low density limit,  $m^* = m$  and  $Z_F = 1$  at  $\rho = 0$ , cannot be explored by the numerical procedures we use and is beyond the range of applicability of the fits (10) and (11). At normal nuclear density  $Z_F \simeq 0.72$  which means a reduction of the effective interaction between quasiparticles by a factor  $Z_F^2 \simeq 0.5$ .

We extend previous calculations of the self-consistent  $T$ -matrix to soft core CDBonn and Nijmegen nucleon–nucleon potentials. We include in the calculation partial waves up to the total angular momentum  $J = 8$ . We present for the first time results on the binding energy for such realistic and detailed parameterizations of the two-body interactions. The reduced binding leads to a harder equation of state, a smaller binding energy and a smaller saturation density than the BHF approximation. The pressure we find is thermodynamically consistent as expected for a conserving approximation. The single-particle energy and the width at the quasiparticle pole come out similarly for different interactions used. It is remarkable that differences in the Hartree–Fock energies and differences in the off-shell behavior of the imaginary part of the self-energy cancel out in the single-particle potential. We present results on the properties of the quasiparticle pole at the Fermi surface. The effective mass is close to the free one and the renormalization factor of the quasiparticle pole is  $Z_F \simeq 0.7$  around the normal nuclear density.

## REFERENCES

- [1] J.P. Jeukenne, A. Leugeunne, C. Mahaux, *Phys. Rep.* **25**, 83 (1976).
- [2] R. Brockmann, R. Machleit, *Phys. Rev.* **C42**, 1965 (1990).
- [3] R.B. Wiringa, V. Fiks, A. Fabrocini, *Phys. Rev.* **C38**, 1010 (1988).
- [4] A. Akmal, V.R. Pandharipande, D.G. Ravenhall, *Phys. Rev.* **C58**, 1804 (1998).
- [5] W.H. Dickhoff, *Phys. Rev.* **C58**, 2807 (1998).
- [6] P. Bożek, *Phys. Rev.* **C59**, 2619 (1999).
- [7] P. Bożek, P. Czerski, *Eur. Phys. J.* **A11**, 271 (2001).
- [8] P. Bożek, *Phys. Rev.* **C65**, 054306 (2002).
- [9] Y. Dewulf, D. Van Neck, M. Waroquier, *Phys. Rev.* **C65**, 054316 (2002).

- [10] R. Machleidt, F. Sammarruca, Y. Song, *Phys. Rev.* **C53**, R1483 (1996).
- [11] V.G. Stoks, R.A.M. Klomp, M.C.M. Rentmeester, J.J. de Swart, *Phys. Rev.* **C48**, 792 (1993).
- [12] L. Kadanoff, G. Baym, *Quantum Statistical Mechanics*, Benjamin, New York 1962.
- [13] G. Baym, *Phys. Rev.* **127**, 1392 (1962).
- [14] N. Hugenholtz, L.V. Hove, *Physica*, **24**, 363 (1958).
- [15] W.H. Dickhoff, C.C. Gearhart, E.P. Roth, A. Polls, A. Ramos, *Phys. Rev.* **C60**, 064319 (1999).
- [16] A. Schwenk, B. Friman, G.E. Brown, *Nucl. Phys.* **A713**, 191 (2003).
- [17] P. Bożek, *Phys. Rev.* **C62**, 054316 (2000).
- [18] P. Bożek, *Phys. Lett.* **B551**, 93 (2002).